Draft version November 20, 2012
Preprint typeset using LaTeX style emulateapj v. 5/2/11

COSMIC MICROWAVE BACKGROUND FILTERS AND THE DARK-FLOW MEASUREMENT.

F. Atrio-Barandela[1], A. Kashlinsky[2] H. Ebeling[3], D. Kocevski[4]

Draft version November 20, 2012

ABSTRACT

Recent measurements of large-scale peculiar velocities from the cumulative kinematic Sunyaev-Zeldovich (KSZ) effect identified a bulk flow of galaxy clusters at $\sim 600 - 1,000$ km s^{-1} on scales of $\sim 0.5 - 1$ Gpc, roughly aligned with the all-sky Cosmic Microwave Background dipole. The signal originates from a residual dipole in the direction of galaxy clusters, at apertures containing zero monopole. Its amplitude increases with the X-ray luminosity of the clusters. The data need to be filtered to remove the primary CMB, thereby increasing the signal-to-noise ratio. Filtering cannot imprint a signal with the mentioned properties at cluster positions, but an inadequately designed and implemented filter can greatly suppress it. We show here that recent studies that failed to detect a large-scale flow indeed used inadequate implementations. These analysis assumed cluster extents and electron-pressure profiles inconsistent with the data. We show that the results from these alternative filters are consistent (although not identical) with our measurement, when filters are normalized to the data. The discrepancies can be traced to the assumptions on cluster profile and extent that reduce the efficiency of the filter and the possible existance of thermal Sunyaev-Zeldovich residual dipoles. The upcoming PLANCK maps, with their large frequency coverage, and in particular the 217GHz channel, will be important to probe the bulk flows as well as to remove spurious dipole signals and further identify the filtering schemes appropriate for this measurement.

Subject headings: cosmology: cosmic microwave background, cosmology: large scale structure of the universe, cosmology: observations

1. INTRODUCTION.

Peculiar velocities are deviations from the uniform expansion of the Universe. In the standard gravitational instability paradigm, they are generated by inhomogeneities in the matter distribution, which in turn are fixed by the concordance ΛCDM model. Measurements of peculiar velocities using galaxies rely on distance indicators to subtract the Hubble expansion, limiting the volume probed by velocity surveys to $\sim 100h^{-1}$Mpc (see Strauss & Willick 1995, Kashlinsky, Atrio-Barandela & Ebeling 2012 for reviews). As an alternative method, Kashlinsky & Atrio-Barandela (2000, hereafter KAB) proposed a specific way to utilise the kinematic Sunyaev-Zeldovich (SZ) effect in clusters of galaxies (Sunyaev & Zeldovich 1970, 1972) to probe large-scale bulk flows. The SZ distortion in the Cosmic Microwave Background (CMB) remains fixed, once it is imprinted by the free electrons of the intracluster gas. It does not depend on distance, making it a very useful tool to detect clusters at high redshift (Planck Collaboration, Planck Early results XXVI, 2011). The SZ has two components: thermal (TSZ), caused by the thermal motions of electrons in the potential wells of clusters, and kinematic (KSZ), caused by the motion of the cluster as a whole with respect to the isotropic CMB rest frame at the cluster location (Birkinshaw 1999). The KSZ effect could be used to trace the velocity field to larger distances than velocity surveys and is dominated by different systematics. It does not require subtraction of the Hubble expansion and it measures motion directly with respect to the CMB frame. The KAB method evaluates the dipole from an all-sky CMB temperature map at the locations of identified X-ray clusters. Since the main contaminant of the component is the primary CMB signal (Haehnelt & Tegmark 1996, KAB), the data need to be filtered to remove the primary CMB; KAB proposed to use a Wiener-type filter for this purpose.

Using a catalog of $\sim$ 700 X-ray-selected clusters and WMAP 3yr data, we uncovered a large-scale flow in the approximate direction of the all-sky CMB dipole, of amplitude $\simeq$ 600–1000 km s^{-1}, and extending to at least $\simeq 300h^{-1}$Mpc (Kashlinsky et al 2008, 2009). This analysis has since been extended to larger scales, using a deeper and larger sample of over 1,200 clusters and 5-yr and 7-yr WMAP CMB data (Kashlinsky et al 2010, Kashlinsky, Atrio-Barandela & Ebeling, 2011). For our largest sample we showed that, at the cluster apertures containing zero CMB monopole, a residual CMB dipole exists which is aligned with the CMB dipole. The dipole amplitude scales with cluster luminosity, proving that the dipole signal is associated with clusters. Since the monopole provides an upper bound to any TSZ dipole caused by an inhomogeneous distribution of clusters in the sky, the measurement could not have originated from the thermal component.

Using publicly available cluster data, Keisler (2009) found a dipole with an amplitude and direction in agreement with our results, but pointed out, simultaneously with Kashlinsky et al (2010), that Kashlinsky et al (2008, hereafter KABKE) had not corrected for the correlation of the residual CMB between WMAP's eight Differencing Assemblies (DA). Keisler concluded that KABKE had underestimated the uncertainties of their measurement and that their

[1] Física Teórica, Universidad de Salamanca, 37008 Salamanca, Spain; atrio@usal.es
[2] SSAI and Observational Cosmology Laboratory, Code 665, Goddard Space Flight Center, Greenbelt MD 20771; Alexander.Kashlinsky@nasa.gov
[3] Institute for Astronomy, University of Hawaii, 2680 Woodlawn Drive, Honolulu, HI 96822; ebeling@ifa.hawaii.edu
[4] Department of Physics, University of California at Davis, 1 Shields Avenue, Davis, CA 95616, USA; kocevski@physics.ucdavis.edu

detection of a large-scale flow was in fact not statistically significant. However, Atrio-Barandela et al (2010, AKEKE) showed that Keisler (2009) had failed to subtract the dipole of the filtered maps outside the Galactic mask, thereby overestimating the error bars of his own measurement by a roughly equal amount. In addition, AKEKE studied the error budget of the KABKE study analytically and numerically and proved that the filter devised by KABKE removes the primary CMB down to the fundamental limit of cosmic variance. It was this highly efficient filtering scheme that allowed a detection of the flow at 3-4σ confidence level, depending on the cluster sample used. All data needed to verify the measurement have been made publicly available[5] for use and examination by the interested reader.

Our results have been challenged in other recent studies. Osborne et al (2011, OMCP) studied the effect of different filters on bulk-flow measurements from WMAP data, and Mak, Pierpaoli & Osborne (2011) applied their filtering scheme to Planck data. When using our filtering scheme as devised by KABKE, OMCP explicitly disprove the Keisler (2009) result by reproducing, in their appendix, the DF dipole at the 2.9σ confidence level. The difference to our $3.5-4\sigma$ result was shown to be due to differences in the catalogs used (Kashlinsky, Atrio-Barandela & Ebeling, 2011) and the limited number of simulations (~ 100) used by OMCP in their analysis of the error budget. They also implemented alternative filters, known as matched filters, designed less to remove the primary CMB anisotropies than to detect radio point sources. With these alternative filters OMCP found no significant dipole and concluded that no evidence of bulk flows was present in the WMAP data. However, OCMP showed their filters to be very insensitive to bulk motions; a sample of ~ 730 clusters moving at velocities of $\sim 4,000-10,000$ km s^{-1} was required to produce a detectable signal. But at such extreme velocities, the motion of individual clusters of mean optical depth $\langle\tau\rangle \simeq 5\times10^{-3}$ should be detectable directly in the original CMB maps without any need for filtering. In another study Mody & Hajian (2012, MH), repeated our analysis using a different type of Wiener filter and concluded that the measured bulk-flow amplitude was "consistent with the ΛCDM prediction". While factually correct, this statement (made prominently in the MH abstract) becomes largely meaningless since the error bars of MH's analysis were about 1,400-2,600 km s^{-1} per velocity component, rendering their methodology unable to discriminate between the concordance ΛCDM prediction and a bulk flow of amplitude $600-1000$ km s^{-1} as measured by KABKE.

The OMCP and MH results have been used repeatedly as evidence against the existence of a DF, without recognizing that spherically symmetric filters can not imprint a dipole signal onto the CMB, exclusively at cluster positions and increasing with cluster X-ray luminosity, but, if implemented improperly, they could remove such a dipole signal. We show below that the latter is indeed the case with the filters used by OMCP and MH. Taking into account the differences associated with filter properties and their effects on the data, we demonstrate that our pipeline recovers measurements with either filter that are compatible with the DF identified in KABKE. The origin of the discrepancy between implementations is that, for clusters, the electron density and electron pressure profiles and their extent in the real and in the filtered data are different while OMCP and MH assume them to be the same. This paper is structured as follows: In Sec. 2 we discuss the properties of filters and their effect on the data. In Sec 3 we compute the CMB dipole at cluster locations on maps filtered with the different filters, and in Sec 4 we discuss the consistency between the different results. Finally, in Sec 5, we present our conclusions.

2. KAB METHOD AND CMB FILTERING

At the positions of clusters, the microwave temperature anisotropies have four main components: the primary CMB, TSZ, KSZ and instrument noise. The subtraction of foreground emission will leave some residuals, but these are negligible compared with the cosmological signal outside the Galactic plane. KAB estimated the CMB dipole at the cluster positions to be

$$a_{1m} = 1\mu K\left(\frac{V_{\rm bulk}}{300\ {\rm km\ s^{-1}}}\right) \pm 3\mu K\left(\frac{N_{\rm cl}}{1000}\right)^{1/2} \pm 0.6\mu K\left(\frac{N_{\rm pix}}{10000}\right)^{1/2} \pm 0.2\mu K\left(\frac{N_{\rm cl}}{1000}\right)^{1/2} \quad (1)$$

where the terms on the right-hand side describe the contributions from the KSZ, the cosmological CMB, noise, and the TSZ, respectively. In this expression, $V_{\rm bulk}$ is the bulk motion of a sample of $N_{\rm cl}$ clusters that occupy a solid angle of $N_{\rm pix}$ pixels in the sky. Combining $N_{\rm DA}$ Differencing Assemblies (DA) at different frequency bands, the noise can be further reduced as $N_{\rm DA}^{-1/2}$. In addition, the TSZ effect can be removed by using its distinctive frequency dependence, or by measurements in increased apertures for non-isothermal clusters. The largest systematic error comes from the intrinsic CMB signal and has two components: (1) a residual dipole left after removing the all-sky CMB dipole from the map, and (2) a sample-variance dipole due to the evaluation of the signal at a small number of pixels containing primary CMB emission. The latter is the largest source of error in eq. (1) (KAB).

To determine peculiar velocities using the KSZ effect, it is necessary to increase the signal-to-noise ratio (S/N) by reducing the primary CMB anisotropy (see eq. 1). Frequency information can not be used to separate the CMB dipole contribution from the signal of interest, the KSZ dipole, since both have the same frequency dependence. However, the CMB dipole will be present at all pixels in the map, whereas the KSZ signal will correlate with the positions of galaxy clusters. Exploiting this property, KAB proposed to use statistical properties of the CMB to design a filter that efficiently removes its contribution while preserving the KSZ component, thereby increasing the S/N of the proposed measurement. To construct such a filter it is important to understand how it affects the dipole signal from a potential bulk flow. Before discussing the properties of different filters we first consider the distribution of the KSZ component in ℓ-space.

[5] http://www.kashlinsky.info/bulkflows/data_public

2.1. *The KSZ signal.*

Our bulk-flow studies were based on an all-sky cluster sample created by combining the ROSAT-ESO Flux Limited X-ray catalog (REFLEX) (Böhringer et al. 2004) in the southern hemisphere, the extended Brightest Cluster Sample (eBCS) (Ebeling et al. 1998, 2000) in the north, and the Clusters in the Zone of Avoidance (CIZA) (Ebeling et al. 2002; Kocevski et al. 2007) sample along the Galactic plane. For simplicity, we restrict our analysis to the most X-ray luminous clusters featuring $L_X[0.1-2.4\ \mathrm{keV}] \geq 10^{44}$ erg s^{-1} and redshifts $z \leq 0.3$. A total of $N_{\rm cl} = 480$ clusters fall outside the WMAP's KQ75 map which masks out the extended Galaxy as well prominent point sources and removes $\sim$29% of the sky. The X-ray emission from each clusters in our sample was fit with a β-model with $\beta = 2/3$. The parameters of this β-model (core radius r_c, central density n_e, and X-ray angular extent θ_X) were derived from the X-ray data, and an estimate of the intra-cluster gas temperature was determined from the $L_{\rm X} - T_{\rm X}$ relation of White et al (1997). From these model parameters we computed the electron-density and electron-pressure profiles. We found that, for the central part of clusters, the amplitude of the TSZ measured from WMAP data differs by less than 10% from the amplitude predicted for our sample (Atrio-Barandela et al 2008). Outside the central region, the amplitude differed from the β-model prediction and was closer to the one predicted by the Komatsu & Seljak (2001) model.

The final cluster sample occupies a less than 1% of the sky. In such a small solid angle, spherical harmonics are not orthogonal, and the spherical harmonic transform redistributes the dipole power at $\ell = 1$ among all multipoles. If we compute the spherical harmonic expansion of the KSZ component, the power for a given multipole ℓ is $(2\ell+1)C_\ell^{\rm KSZ} = \sum_m |a_{\ell,m}^{\rm KSZ}|^2$, where the $a_{\ell,m}^{\rm KSZ}$ are the spherical harmonic transforms of the KSZ component at $N_{\rm cl}$ locations in the sky. The integrated dipole signal then gives the contribution of all multipoles $i \leq \ell$ to the dipole present in the map:

$$S^2(\ell) = \frac{1}{4\pi}\sum_{i=2}^{\ell}(2\ell+1)C_\ell^{\rm KSZ}. \tag{2}$$

Prediction of the KSZ power spectrum and of $S(\ell)$ requires knowledge of the electron-density profile for all clusters in any given sample, i.e., data which are not yet available. To simplify the problem, we will assume that all clusters subtend the same angle and move coherently in the direction $(l, b) = (270^\circ, 30^\circ)$ with arbitrary amplitude. In Figs 1a and 1b, we plot the power and the integrated dipole signal $S(\ell)$, respectively, for identical clusters of angular radius $30'$, $15'$and $10'$. Fig 1a shows that the lowest multipoles have the largest amplitude, and that power is transferred preferentially to odd multipoles. Because the clusters in our sample occupy a very small solid angle, power is also transferred to much higher multipoles. Fig 1b shows that less than 10% of the signal remains at $\ell = 1$; the bulk of the signal is contained in the range $\ell = 1 - 300$. The angular extent of the clusters in the sky determines the distribution of the KSZ signal in ℓ space. The actual signal will be a combination of the contribution from resolved ($15'$-$30'$) and unresolved ($10'$) clusters, with clusters of different mass contributing at different relative weights. For illustration, in Fig 1b the solid black line represents the W1 filter used by Osborne et al (2011) discussed below, showing that this filter preferentially probes the scales corresponding to $300 \leq \ell \leq 800$ while most of the signal is below $\ell = 300$.

Since CMB temperature anisotropies are spatially isotropic and follow a Gaussian distribution about their mean, the angular correlation function $C(\theta)$ contains all the relevant statistical information of the temperature field. Because of isotropy, in ℓ-space, the filter can only depend on ℓ but not on m. If $\Delta T = \sum_{\ell m} a_{\ell m} Y_{\ell m}$ and $F(\theta) = (1/4\pi)\sum_\ell (2\ell+1)F_\ell^2 P_\ell(\cos\theta)$ are the expansions of the temperature map in spherical harmonics and of the filter in Legendre polynomials, respectively, then the filtered map is given by

$$F \star \Delta T = \sum_{\ell m} F_\ell a_{\ell m} Y_{\ell m}\,. \tag{3}$$

KAB discussed two types of filters: (1) global filters that operate over the whole sky, and (2) local filters that subtract the primary CMB signal only at the positions of clusters. All filters presented in the literature are spherically symmetric (i.e., they depend only on ℓ) and can be implemented globally and/or locally. As shown in Fig. 1, filters which are cut off at $\ell \lesssim 200 - 300$ will, in ℓ-space, remove the KSZ dipole, $C_\ell^{\rm KSZ}$, together with the cosmological CMB signal and noise and do not necessarily increase the S/N. In the following we briefly describe the filters that have appeared in the literature.

2.2. *The KAB filter.*

The KAB filter was specifically designed to remove the primary CMB of the measured cosmological model. The filter is of the Wiener type and was constructed to minimize the contribution from the cosmological signal in the filtered maps in the presence of noise, $\mathcal{N}$, i.e. it minimizes $\langle(\Delta T - \mathcal{N})^2\rangle$ (Kashlinsky et al 2009). In ℓ-space the filter is given by

$$F_\ell^{\rm KAB} = \frac{C_\ell^{\rm sky} - C_\ell^{\Lambda{\rm CDM}} B_\ell^2}{C_\ell^{\rm sky}}\,, \tag{4}$$

where $C_\ell^{\rm sky}$ is the actual realization of the radiation power spectrum in the sky that includes noise, TSZ, KSZ, foreground residuals, and primary CMB; $C_\ell^{\Lambda{\rm CDM}}$ is the power spectrum of the ΛCDM model that best fits the data, and B_ℓ is the antenna beam for a given DA. Since the quadrupole and octupole are aligned with the dipole, the KAB

filter is set to zero for $\ell \leq 3$ to avoid any cross-talk from the corresponding large angular scales that could mimic a dipole. Atrio-Barandela et al (2010) proved that this filter removes the intrinsic CMB signal down to the fundamental limit imposed by cosmic variance. In this sense, the filter is optimal; no other filter can remove the intrinsic CMB signal better, and improvements on the S/N ratio must come by restricting the analysis to some specific range of multipoles.

Fig. 2a shows the KAB filter for the W1 DA. The filter has structure at all multipoles and therefore preserves the KSZ signal better than a simple high-pass or band-pass filters that remove the power outside a given multipole range.

2.3. *OMCP filters.*

An alternative filtering scheme was used by Osborne et al (2011). OMCP employed matched filters that are well suited to distinguish point sources from a background signal, provided the point source profile is known. Their Matched Filter (MF) is defined as

$$F_\ell^{\rm OMCP} = \frac{B_\ell}{(C_\ell^{\Lambda{\rm CDM}} + C_\ell^{\rm TSZ})B_\ell^2 + N_\ell}\,, \tag{5}$$

where $C_\ell^{\rm TSZ}$ and N_ℓ are the power spectrum of the TSZ effect and of the white and homogeneous instrumental noise, respectively. As in Eq. 4 above, B_ℓ is the antenna beam for a give DA. They also considered a modification of this filter, named Unbiased Multifrequency Matched Filter (UF), to remove the TSZ contribution. These filters require the electron density and electron pressure profiles to be known. Assuming all clusters to be unresolved, OMCP approximated cluster profiles by the WMAP beam function. If this assumption were correct, the TSZ and KSZ signal would be erased equally since they are proportional to each other, and this information could be used to calculate the fraction of KSZ lost due to filtering. However, *since clusters are not isothermal (as demonstrated, e.g., by Atrio-Barandela et al 2008), the electron density and pressure profiles are in fact different,* enabling filters disregarding this fact to potentially erase the KSZ signal much more efficiently than the TSZ contribution.

We will illustrate this for the MF used by OMCP and will handle any possible TSZ contamination in the same way as for other filters. In Fig. 2b we plot the OMCP filters for eight WMAP DA, corresponding to the Q (green), V (blue) and W (red) bands. These filters are effectively band-pass filters, removing all power below $\ell \lesssim 200 - 300$ and above $\ell \sim 800 - 1000$. The damping tails are dominated by the beam function. OMCP normalized their filters such that the KSZ dipole amplitude in the unfiltered and in the filtered maps were the same. Again, implicit in this normalization cluster profiles and extents are required to be known to determine by how much the filter dilutes or boosts the signal. We do not make any assumption of this type and will use the data to normalize the filters (see Sec. 3.1 below for details).

2.4. *Mody-Hajian filter*

Mody & Hajian (2012) used a Wiener filter designed to remove, together with the intrinsic CMB, the TSZ and instrument noise contributions, leaving only the KSZ component in the data. Their filter is defined by

$$F_\ell^{\rm MH} = \frac{C_\ell^{\rm KSZ} B_\ell^2}{[C_\ell^{\Lambda{\rm CDM}} + C_\ell^{\rm TSZ}]B_\ell^2 + N_\ell}\,, \tag{6}$$

where $C_\ell^{\rm KSZ}$ is the power spectrum of the KSZ contribution, and the other terms have the same meaning as in eqs. (4, 5). This filter neglects the inhomogeneities in the instrumental noise, and to construct it MH need to know $C_\ell^{\rm KSZ}$, the same quantity they want to measure. This means MH need to 1) specify the cluster distribution on the sky, 2) assume for all clusters an electron density profile, and 3) fix the cluster extent, quantities that have yet to be measured from the data. Therefore, the real shape of their filter is unknown. Statistical studies of this filter conducted with a cluster template that matches the KSZ signal in the simulated data will overestimate its performance and understimate the final error budget.

In Fig. 2c we plot the MH filter for two different assumptions. The black solid line takes all clusters to have an extent of $10'$, while the blue line assumes a angular radius of $15'$; both are convolved with the beam of the W1 DA. The filter is normalized to a KSZ dipole in the Z-direction with an amplitude of 10μK; convolution with the beam reduces the amplitude to $\sim 5\mu$K. These two curves can be thought as two extreme cases of what the actual MH filter might be. Taking into account that very few clusters are resolved at WMAP W band, in the subsequent discussion we will only consider the MH filter constructed with clusters of $10'$ angular radius.

2.5. *The effect of filtering on the data.*

Filtering not only removes the intrinsic CMB component, it also modifies the KSZ signal. As a result, the cluster extent and profile will be affected by the filter, including the sign of the KSZ dipole component at the final aperture (Kashlinsky et al 2011). If $T(\theta) = (1/4\pi)\sum(2\ell+1)T_\ell P_\ell(\cos\theta)$ is the cluster profile, then the profile of a cluster seen with an antenna beam B_ℓ and convolved with a filter F_ℓ is given by

$$(F \star T)(\alpha) = A\sum(2\ell+1)F_\ell T_\ell B_\ell P_\ell(\cos\alpha)\,, \tag{7}$$

where A is a normalization constant to be determined and $\star$ represents convolution. In Figs. 2d–f we plot the filter profile in real space. If a cluster occupied a single pixel in the unfiltered map, Figs. 2d–f would represent its profile in

the filtered map. We use the MH filter constructed with clusters of $10'$. The filtered cluster profile is more extended than the original profile and not always positive: it will be non-zero up to $40'$, feature a first zero-crossing at 13–$24'$ and a first minimum at 17–$30'$. By cutting power in ℓ-space, filtering makes the function $F_\ell T_\ell$ narrower than T_ℓ. Therefore, in real space, the profile convolved with the filter, $F \star T(\theta)$, is wider than the original profile, $T(\theta)$. *This point was missed by OMCP who used only the central cluster pixels, and by MH who assumed that clusters in the filtered maps have the same extent as in real maps.*

Since WMAP has lower resolution than Planck, and WMAP data are noisier, the WMAP-based results in Kashlinsky et al (2010) and (2011) were obtained by evaluating the dipole at a fixed aperture of $\sim 25'$ radius. To assess the impact of this choice, it is informative to compute the measured cluster profile in the filtered map given in eq. 7, averaged over a disc of angular radius ρ:

$$\langle F \star T \rangle_\rho = \frac{1}{\rho^2} \int_0^\rho (F \star T(\alpha)) d\cos\alpha \,. \tag{8}$$

In Fig. 2g–h we plot the above average as a function of the disc angular radius ρ for the KAB, OMCP, and MH filters, respectively. To avoid overcrowding the plots, we only represent the Q1, V1 and W1 DA's. Since the KAB filter is the one that preserves the most power, the signal of an unresolved source vanishes around $20'$, while it extends to about $30'$ for the OMCP filters, and goes well beyond $40'$ for the MH filter. These extents correspond to clusters that are unresolved subtending a single pixel on the sky; for resolved sources the signal will spread to apertures of even larger radii.

3. MEASURING BULK FLOWS IN WMAP DATA WITH THE KAB METHOD.

To measure the dipole at cluster locations in the CMB maps as filtered by KAB, OMCP, and MH our pipeline proceeds as follows:

1. For each DA, the data are multiplied by the WMAP7 extended mask KQ75. Then, monopole, dipole, and quadrupole are subtracted from the regions outside the mask. Next, we apply a Legendre transformation to the data in order to compute the $(a_{\ell m})$ multipoles. The power lost due to masking is corrected by multiplying each multipole by $f_{\rm sky}^{-1/2}$, where $f_{\rm sky}$ is the fraction of the sky outside the mask.

2. The a_{lm} terms are multiplied by the filter F_ℓ before transforming them back into real space to produce the filtered map.

3. The monopole and dipole outside the mask are removed from the filtered maps. *Keisler (2009) failed to take this important step, which lead him to overestimate the error bars.*

4. Dipoles are computed at the cluster positions for different apertures. At each cluster position, we estimate the monopole and dipole over a fixed aperture of radius ρ, for all clusters. Of all the dipole values, we select the dipole measured at *zero monopole aperture* as the one least contaminated by a TSZ dipole.

By computing monopoles and dipoles at the positions of clusters we have control over both SZ components: the monopole is dominated by the TSZ effect and provides an upper limit to any TSZ dipole that originates from the inhomogeneous distribution of clusters on the sky. Hence our choice of aperture: at the zero-monopole aperture, any resulting dipole associated with the respective cluster has to be due to the KSZ effect. The largest contribution to this dipole comes from the zero-order moment, which is the average motion of all the clusters in the sample. Kashlinsky et al (2010) obtained their results with an aperture of $\rho \sim$ 25–$30'$. At those radii, we detected a $3-4\sigma$ dipole signal. The absence of a monopole in these apertures ruled out any TSZ contribution. We also showed that the measured dipole scaled with the TSZ monopole measured at the cluster centers and, therefore, had to be associated with clusters. Since the TSZ is diluted faster than the KSZ signal, the electron density (KSZ) profile must be more extended than the electron pressure (TSZ) profile. This was empirically anticipated in Atrio-Barandela et al (2008), where we demonstrated that clusters cannot be represented by an isothermal β-model outside their central regions. The Komatsu & Seljak (2001) model provided a much better fit. In this model, hydrostatic equilibrium requires that the cluster temperature falls with radius (for a full discussion on this point, see Kashlinsky et al 2009, Kashlinsky et al 2012).

Due to the different functional form of the three filters, the KSZ power will be differently altered by each filter. In order to compare the results, the dipole measured in temperature units needs to be converted to velocity units. This requires a detailed knowledge of the density profile and extent of individual clusters and how they are affected by the filter. As an alternative, we will use the results presented in Figs. 2d–f to normalize homogeneously the filtered maps, as described below.

3.1. *Filter normalization.*

In their central regions, relaxed clusters are close to isothermal (Pratt et al 2011). If the electron pressure and electron density are proportional to each other we can assume that the dilution of the TSZ and KSZ components by the filter would be similar. By measuring the TSZ effect on a very narrow region around the cluster center in the original and in the filtered maps, we could determine this dilution factor. To be precise, we will assume that close to the center the cluster profile (convolved with WMAP beam) before and after filtering can be expressed as

Cluster Sample		N_{cl}	f_{sky}[10']	TSZ[5']/μK				R^F[5']		
				WMAP	KAB	OMCP	MH	KAB	OMCP	MH
I	$L_X > 1$, $z < 0.3$	480	10^{-3}	-24 ± 3	-15 ± 4	-69 ± 21	-0.047 ± 0.010	1.7±0.3	0.37±0.06	530±80
II	$L_X > 1$, $z < 0.16$	285	6×10^{-4}	-28 ± 6	-19 ± 6	-88 ± 30	-0.053 ± 0.012	1.6±0.4	0.33±0.06	540±60
III	$L_X > 2$, $z < 0.3$	272	6×10^{-4}	-34 ± 9	-20 ± 4	-91 ± 24	-0.069 ± 0.012	1.7±0.2	0.37±0.05	500±120
IV	$L_X > 2$, $z < 0.16$	115	2.4×10^{-4}	-40 ± 8	-31 ± 4	-145 ± 38	-0.1 ± 0.02	1.27±0.14	0.28±0.4	430±80

TABLE 1
Different cluster samples considered in this work and some of their properties. X-ray luminosities are in units of 10^{44}ergs/s and temperatures in μK.

$T(\theta) = T_o(1 - 1/2(\theta/\sigma)^2)$ and $F \star T(\theta) = T_o^F(1 - 1/2(\theta/\Delta)^2)$. For an unresolved source, σ is the WMAP antenna beam width while Δ is the characteristic extent of clusters in the filtered map. If we average the cluster profile before and after filtering on a disc of radius $\rho \leq \sigma, \Delta$, then R^F, defined as the ratio of the two averages, is

$$R^F = \frac{\langle T \rangle_\rho}{\langle F \star T \rangle_\rho} = \frac{T_o(1 - 1/2(\rho/\sigma)^2)}{T_o^F(1 - 1/2(\rho/\Delta)^2)}\,, \tag{9}$$

This ratio is an observable quantity. It can be derived from the data by averaging the temperature anisotropy at cluster positions over aperture of radius $\rho = 5'$. It will be different for each filter and for each band. To determine the dilution factor (T_o/T_o^F) from R^F requires to determine the characteristic angular extents of clusters, σ, Δ, *before and after filtering*. If $\sigma = \Delta$ then $R^F = (T_o/T_o^F)$. Within this approximation, by multiplying each DA by its corresponding renormalization factor R^F, all maps are renormalized to have the same monopole over apertures of radius $\rho = 5'$ and equal to the monopole of the original WMAP data. With this normalization, the KAB, MH and OMCP filtered maps have similar power, enabling direct comparison of monopoles and dipoles.

Note that this normalization is uncertain in several aspects: the dilution factor R^F is different for different cluster samples and for different DA's. The averages at the cluster locations contain not only the TSZ monopole but also CMB residuals and noise; depending on the filter, beam shape and beam asymmetries. All these effects give rise to differences between the DA's within the same band. To reduce these uncertainties, we will define a different R^F for each cluster configuration and each band, taking the average over DA's. We will then quote the results for the W-band, where the average is over four DA's, but the results including all other bands are very similar.

3.2. *Filtered maps.*

The W1 DA's filtered with the KAB, OMCP and MH filters, normalized using the dilution coefficient of our full cluster sample are shown in Fig 3. In the left column and from top to bottom we plot the KAB, OMCP and MH filtered maps. The KAB filter contains more structure at large scales since it preserves power below $\ell = 300$. The OMCP filtering erases all power at $\ell \lesssim 200 - 300$ and the resulting filtered maps show no large scale features. Since maps have the same normalization, we can subtract them to compare the differences between filters. In the right column, we plot the difference between the KAB and OMCP (top panel) and between the OMCP and MH (middle panel) filtered maps. The difference between KAB and OMCP is dominated by the large angular scales that survived the KAB filter. The differences between KAB and MH are larger, with a more complex pattern since both filters preserve power at all scales, and is not shown. In the middle panel, the differences between OMCP and MH filtered maps are dominated by small scale features and noise. Finally, in the bottom left panel we plot the position of our 480 clusters with X-ray luminosity $L_X[0.1 - 2.4KeV] \geq 10^{44} erg/s$ and $z \leq 0.3$ that are outside the KQ75 mask. For easier view, all clusters have been assigned a size of 1.5°.

3.3. *Dipoles.*

We now compare the efficiency of the three filters discussed in this article by measuring the dipoles at the cluster locations. We divide our catalog into four samples. The selection criteria and cluster properties are given in Table 1, ordered by decreasing number of clusters. The samples are not independent; clusters with $z \leq 0.16$ are included in the sample $z \leq 0.3$ and similarly with the two luminosity subsamples. Also, we give the number of clusters N_{cl} for each sample and the fraction of the sky f_{sky} occupied if all clusters had the angular size of $10'$. The next columns list the monopole over an aperture radius $5'$in the original WMAP data and in the KAB, OMC and MH filtered maps. The value is the mean of the four W-band DA and the error bar is the rms dispersion of the four measurements. These results do not change if the Q and V bands are included. Finally, we also give the dilution factor R^F for the W-band and the rms dispersion within the four DA. From Table 1, the dilution factor is 1.3-1.7 for the KAB filter, ~ 500 for the MH filter, while the OMCP filter boosts the signal (not the signal/noise) by a factor of ~ 3.

We computed dipoles for the four cluster samples of Table 1 and different apertures: $\rho = [5, 10, 20, 30, 40, 50, 60]$arcmin. As shown in the Table, the dilution factors are different for each cluster sample. Dipoles are normalized by the factor corresponding to each cluster configuration. If the dilution factor of the TSZ and KSZ signals were the same, the renormalized dipoles would be the original dipole of the unfiltered map. In Figs. 4a-c we plot the three dipole components (X,Y,Z) for the four cluster samples of Table 1, versus the monopole. In all the filtered maps (KAB, OMCP and MH) monopoles and dipoles were measured over aperture radius $30'$, that roughly corresponds to the zero monopole aperture of the KAB filter. Crosses, diamonds and triangles correspond to the KAB, OMCP and MH filters,

Cluster	KAB				OMCP				MH			
Sample	M/μK	D/μK	ℓ/deg	b/deg	M/μK	D/μK	ℓ/deg	b/deg	M/μK	D/μK	ℓ/deg	b/deg
I	-0.9± 0.7	5.8±1.7	289±32	36±16	-2.7± 0.6	3.2±1.3	243±38	2±31	-7.4± 1.4	8.2±2.1	223±18	1±13
II	1.2± 0.4	5.7±1.6	249±17	11±19	-2.1± 0.5	3.8±1.5	262±57	2±37	-6.9± 1.0	10.8±3.0	242±14	0±24
III	-2.4± 1.6	9.6±1.1	257±14	41±7	-4.8± 1.2	5.6±1.4	214±19	-15±15	-12.5± 2.0	14.5±3.3	206±15	-13±11
IV	1.0± 1.0	11.1±1.5	231±9	21±7	-3.4± 1.0	4.2±1.3	205±32	-16±24	-10.5± 2.1	15.7±3.1	201±12	-13±11

TABLE 2
Monopoles and Dipoles for different cluster samples and filters, computed with an aperture of $\rho = 30'$.

respectively. The different cluster samples can be distinguished by the color of the error bars. Black, blue, red and green correspond to the cluster samples listed in Table 1 with decreasing number of clusters. Like for the monopole, dipoles are averages of the four W DA's and the error bar is the dispersion within these DA's. The results do not change appreciably if the Q and V bands were added. The error bars are somewhat larger than in our previous studies since now they include the uncertainty of the renormalization coefficient.

In Figs. 4 we can see that while the residual TSZ monopole in the KAB filtered maps (crosses) is in the range $(-3, 2)\mu$K, compatible with zero, it still remains at a significant level for the MH and OMCP filters. Their monopoles are in the range $(-13, -7)\mu$K for MH (triangles) and $(-5, -2)\mu$K for OMCP (diamonds). This reflects the fact that *clusters are more extended for these two filters than for the KAB filter*. The MH filtered maps give the largest monopoles so the measured dipole could have a strong TSZ contribution. The dipoles measured at the OMCP filtered maps have a small amplitude. The three filters show a certain degree of consistency on the value of the Y-component. This component is always negative for all filters and all cluster configurations. This is in agreement with the DF results, where we determined a negative Y-component, a smaller amplitude positive Z-component and the error bar was too large to get any reliable measurement of the X-component.

To quantify the degree of consistency between the three dipoles, in Table 2 we quote the amplitude of the monopole (M) and dipole (D) and the galactic longitude (ℓ) and latitude (b) of the dipoles represented in Fig 4. Error bars are the average and dispersion of 10,000 realizations of moduli and directions derived from the three dipole components $(D_i \pm \sigma_i)$ with $i \equiv (X, Y, Z)$, asuming the realizations to be gaussian distributed with dispersions σ_i around the measured values D_i. The direction of the OMCP dipoles are within 1σ of both the KAB and MH dipoles, but KAB and MH dipole directions are not in such close agreement. With respect to the amplitude, the KAB dipoles have an amplitude about a factor of ~ 2 larger than OMCP dipoles and ~ 1.5 smaller than the MH dipoles. Remarkably, in the three cases the dipole is largest for the clusters with $L_X > 2 \times 10^{44}$erg/s, corresponding to the cluster samples III and IV.

To correct for the effect of the TSZ dipole, we compute the dipoles at the OMCP and MH filtered maps for bigger apertures. We choose $\rho = 50'$ for the OMCP filter and $\rho = 60'$ for the MH filter. At those apertures, the residual monopoles are almost negligible. In Figs. 5a-c we plot the three components of the dipole. For comparison, we also included the results of the KAB filter at $\rho = 30'$. Now the spread in the X-axis is much smaller, indicating that in all cases we are close to the zero monopole aperture. In Figs. 5d-f we plot the previous dipoles, measured at the zero monopole aperture, versus the monopole at $10'$. The three filters show some agreements and some discrepancies: the X-component shows a clear scaling with the TSZ monopole for all filters and all cluster configurations; the Y-component shows scaling for the KAB filter (crosses) and the MH filter (triangles); for the OMCP filter the value is roughly constant at $D_Y = -2\mu$K; finally, the Z-component is compatible with zero for the MH and OMCP filter and different from the KAB filter that shows a positive contribution of different amplitude for the different cluster configurations.

3.4. *From temperature to velocity units.*

From X-ray observations we have derived the $\beta = 2/3$ isothermal cluster model fits to the clusters in our catalog. We can compute the electron density profile, assuming the gas to be distributed like a β-model out to the cluster outskirts. Using the theoretical profiles we can compute the renormalization factors. We found them to be $R^{KAB} = 1.82 \pm 0.05$, $R^{OMCP} = 0.33 \pm 0.06$ and $R^{MH} = 440 \pm 60$. These values are in resonable agreement with the results of the cluster sample I in Table 1. With the data of our catalog we can predict the amplitude of the KSZ dipole in the original WMAP data. The KSZ dipole is $\Delta T_{KSZ} = -T_0 \tau (v/c)$ with τ the projected electron density along the line of sight, v the bulk flow velocity of our cluster sample, c the speed of light and T_0 the CMB blackbody temperature. If we assume that all clusters in our sample have the same angular extent of $10', 15'$ then the average optical depth for our $\beta = 2/3$ clusters is $\langle \tau \rangle = (1.2, 0.97) \times 10^{-3}$. A bulk flow of amplitude 600 km/s would give rise to a dipole of $D = 6.5, 5.3\mu$K. For our cluster sample I, the measured value of the KAB filter is within this range, the OMCP filters is within the 2σ and the MH filters within the 1σ confidence level. Using these results, we can translate the results of Table 2 from temperatures to velocities. For example, using the value $D = 6.5\mu$K, corresponding to clusters of $10'$, the bulk flow velocity of our sample I, in each filter is:

$$V_{bulk}^{KAB} = 560 \pm 160 km/s\,, \quad V_{bulk}^{OMCP} = 310 \pm 130 km/s\,, \quad V_{bulk}^{MH} = 793 \pm 200 km/s\,, \tag{10}$$

These results need to be taken with some caution. The OMCP dipoles and more certainly the MH dipole at $30'$given in Table 2 could have a non-negligible TSZ contribution; also, the error bars have been computed as the dispersion

among the DA's. This ignores the contribution coming from CMB residuals correlated across different bands. Error bars computed over 100 cluster realizations outside the known positions of clusters are 20-40% larger. This contribution is negligible for the OMCP filter since it removes all large scale power, where the CMB residual is largest and it is not very significative for the MH filter for the same reason. A statistically more meaningful comparison would require a study of error bars as detailed as AKEKE for all filters. At present, this study is not adequate for the OMCP and MH filters since WMAP data does not have enough frequency information to remove any TSZ dipole.

Notice that the KAB filter gives amplitudes and directions that are close to the CMB dipole. The amplitude in km/s is smaller than in our previous work (see discussion of this systematic uncertainty in Kashlinsky et al 2009, Kashlinsky et al 2011). Our earlier estimated conversion factor $C_{1,100} = (V_{100}/D)$ from temperature D to velocity $V_{100} = 100$ km/sec went from $C_{1,100} \simeq (100km/s)/1\mu K$ in unfiltered maps to $C_{1,100} \simeq (100km/s)/0.3\mu K$ in the KAB filtered maps. These conversions were obtained assuming that clusters were well described by the isothermal β-models and correspond to a normalization $R^{KAB} = 3.3$, instead of $R^{KAB} \simeq 1.7$ of Table 1.

Let us next discuss the reasons why different filters can give results that are not in full agreement with the others.

4. ARE THE RESULTS CONSISTENT?

All the measured quantities in Figs. 4 and 5 have been corrected by the dilution factor R^F given in eq. (11). Ideally, the quoted values would match the monopoles and dipoles present in the original (unfiltered) maps. Taking the error bars at face value, the results presented in Table 2 indicate that the KAB, OMCP, and MH filters detect dipoles with a high level of significance, but the amplitudes and directions of these dipoles, while mutually consistent, are not in perfect agreement. Since filters operate differently in spherical-harmonics space, there are several effects that can reduce their efficiency.

4.1. *On the efficiency of filters*

There are several aspects that explain why the OMCP and MH filters could be less efficient than KAB in detecting bulk flows. First, the OMCP and MH filters assume that cluster profiles and extents are known. Both filters use the cluster pressure (TSZ) profile to construct the electron density (KSZ) profile: the MH filter does this explicitly since it requires $C_\ell^{\rm KSZ}$ to be known, whereas the OMCP filter makes a similar assumption implicitly by adopting the notion that clusters are unresolved and their profile given by the WMAP beam. We have shown that all filters yield dipoles that are statistically significant at the apertures corresponding to zero monopole and which are thus dominated by the KSZ effect. It follows that the KSZ profile (in the filtered maps) has to be more extended than the TSZ profile. Filters are later normalized to predict the dipole present in the original map. Since filters remove intrinsic CMB and noise, they would also remove TSZ and KSZ contributions. If the KSZ is more extended than the TSZ component, it will be modified more heavily, and hence reconstructing the missing KSZ using only the TSZ part will underestimate the power lost in the KSZ component. Since our normalization procedure uses TSZ monopoles at $5'$, it does not correct for this effect and does not improve the filter's efficiency.

This aspect can be better illustrated with the OMCP filter. Since this filter effectively removes power at all scales above one degree, unlike the KAB filter which preserves power at all scales, it can be applied to the full sky or to small patches around clusters. As an example, we will use the OMCP filter for the W1 DA. In Fig. 2e we see that the filter is positive at the origin, negative at 15–$25'$, and close to zero elsewhere. In real space, the filter will thus average the CMB data on a disc of radius $\sim 15'$ and subtract the average from an annulus of $\sim 15' - 25'$ around the cluster, as has been suggested originall in KAB (see also Fig. 2d). If the cluster is confined to the inner $15'$, the average from the annulus provides an estimate of the CMB contribution in this region. Subtracting this contribution will not alter the KSZ signal. However, if the cluster extends beyond $15'$, the subtraction will reduce the cluster optical depth τ. Estimating the size of this effect requires the cluster profile and extent to be known. We have carried out this test in real space using the Komatsu & Seljak (2001) model. At $30'$, correcting the KSZ using the TSZ profile would reduce the KSZ between 10 and 20%. If, however, the cluster parameters are not known, and the correction is performed using a profile with a concentration parameter unmatched to the cluster, the error grows up to 50%. This could explain the discrepancy in the amplitudes measured by the OMCP and the other two filters. The results obtained with the MH filter are also rather uncertain since this filter can only be constructed if the KSZ power spectrum is known. For instance, we have assumed all clusters to have identical optical depth and angular extent, and have given equal weight to all clusters, while in reality more massive and more extended clusters would contribute more, an effect that could have an strong influence on the direction of the measured dipole.

Biases, while common to all filters, are more severe for the OMCP and MH filters than for the KAB filter. First, if the dipole is computed within an aperture containing a significant monopole component, the measured signal will contain a TSZ dipole contribution that can only be separated using frequency information. The OMCP and MH filters require much larger apertures and thus probe out to radii at which the residual monopoles are consistently negative for the Y-component. Second, the extent of the cluster changes from one filtered map to another. For the more extended clusters, removing the monopole and dipole outside the KQ75 mask in the filtered maps would also erase a larger fraction of KSZ dipole (or any other dipole). Finally, our normalization enables us to compare dipoles measured from different filters, although we emphasize the approximate nature of such a comparison. Apertures of $5'$ occupy very few pixels and sample variance is large; contamination from noise and CMB residuals is non-negligible; finally, the dilution factor depends on the properties of the clusters in our sample. We had assumed in Sec 3.1 that clusters have the same extent in the original and in the filtered maps. This assumption underestimates the true dilution factor, and the bias is largest for the filters in which clusters are more extended.

We now analyze the uncertainty of our normalization in more detail. For our cluster sample IV, the monopole at $10'$ is $(-25, -29, -35)\mu$K for the KAB, OMCP, and MH filters (see green symbols in Fig 5d), with an uncertainty of about 30%. The uncertainty increases for larger apertures. For an unresolved source, we can make a conservative estimate. Figs. 2d–f indicate that the spread of a point source in the filtered map Δ is $\Delta^{\rm KAB} \simeq 0.8\Delta^{\rm OMCP} \simeq 0.6\Delta^{\rm MH}$. If we take $\sigma = \Delta^{\rm KAB}$ and $\rho = 30'$ then eq. (eq:normalization) gives

$$R^{\rm KAB} = \frac{T_o}{T_o^{\rm KAB}},\ R^{\rm OMCP} = 0.75\frac{T_o}{T_o^{\rm OMCP}},\ R^{\rm MH} = 0.63\frac{T_o}{T_o^{\rm MH}}\ , \tag{11}$$

that is, if T_o is the monopole of the TSZ in the original data and T_o^F the same magnitude in the filtered map. Then, by assuming $\Delta^F = \sigma$ we underestimate the dilution factor of the OMCP filter by 25% and of the MH filter by an even greater 37%, compared with the KAB filter. If $\Delta^{\rm KAB} = 1.1\sigma$ then $R^{\rm KAB}$ underestimates the true factor dilution factor of the KAB filter by 14%, of the OMCP filter by 30% and of the MH filter by 40%. The correction of a 25-40% of dipoles measured at $\sim 30'$ aperture is probably larger. This is the level of uncertainty on the TSZ monopole at $10'$when, by construction, all filters have the same amplitude at $5'$ and the uncertainty increases with aperture.

In general, the discrepancies between the results obtained for different filters as described above can be traced back to our present ignorance of the individual cluster profile and extent. Without detailed information of these profiles, we can not fully quantify the loss of efficiency. However, all effects described above bias the results obtained with the OMCP and MH filters more than those measured with the KAB filter since (a) clusters are more extended for the former filters and (b) they require the cluster profile and extent to be known. This is not the case for the KAB filter, which was designed to remove the intrinsic CMB signal down to the limit imposed by cosmic variance (see AKEKE) and which does not require specific assumptions about the cluster profile or extent. As the KAB filter is the least biased in all aspects, one must conclude that its results are the most reliable of the three filters.

4.2. *Comments on previous results.*

All filters discussed in the literature are spherically symmetric. At each ℓ, the phases of the $(2\ell + 1)$ different multipoles are preserved. Hence, such filters cannot generate a dipole at zero monopole. If not carefully chosen and implemented, filters can, however, erase the dipole signal that has been detected in the data at (currently) 3.5–4σ significance. The purpose of this article was to show that the OMCP and MH filters indeed detect a dipole signal in WMAP data that is compatible with the KABKE results and those of our subsequent studies. For completeness, we would like to point out possible reasons for the failure of OMCP and MH to detect this signal in their published analyses.

As described in the introduction, OMCP implemented two multi-frequency matched filters utilized by them for the detection of the KSZ effect. They measured the dipole at the position of 736 clusters of galaxies and found no significant KSZ signal. They introduced two filters: the one discussed in this article, with no spectral dependence, termed Matched Filter (MF), and a simple modification that utilizes the spectral properties of the KSZ and TSZ signals to remove the TSZ bias, termed Unbiased Filter (UF). OMCP tested the performance of their two filters using simulated maps with the full cluster sample. Their filters start to recover the input velocity only at speeds $V_{\rm bulk} \simeq 3000$ km s^{-1} for the MF and $V_{\rm bulk} \simeq 10^4$ km s^{-1} for the UF. For massive clusters like Coma, the optical depth at the center of the cluster ranges from $\tau \sim 0.002$ to 0.004 after convolution with the WMAP beam of the highest resolution; the average mean optical depth of the clusters used by OMCP is stated by the authors to be $\langle\tau\rangle \simeq 4.9 \times 10^{-3}$ (Sec. 4.5 of OMCP). At those speeds, the expected temperature anisotropy would be $\Delta T = 110\mu K(\tau/0.004)(V_{bulk}/3000$ km s$^{-1})$. *A dipole of this amplitude would be measurable in the original data and for each individual massive Coma-class cluster.* The same effect is even more pronounced for the UF. Clearly, OMCP's implementation of their filters did not increase the S/N but strongly reduced it, to the extent that OMCP could not have detected a CMB dipole corresponding to velocity of $\sim 600 - 1000$ km s^{-1} given the larger error bars of their analysis.

In addition, OMCP fitted the dipole only at the central cluster pixels because their filters were optimized to reconstruct the source amplitude if the source was centered on that pixel (Mak et al 2011), ignoring the fact that clusters in the filtered maps are much more extended than in the original maps (see Fig. 2d–i). When instead dipoles are computed within apertures of $30'$ radius, the OMCP MF filter recovers a dipole, albeit with a smaller amplitude. Their UF filter performed even worse and was thus not studied here. Its failure can be traced to the chosen cluster profiles. In addition to not choosing an aperture of appropriate size, OMCP assumed the KSZ and TSZ cluster profiles to be identical and unresolved. Hence, any filter that efficiently removes the TSZ effect will also remove a substantial part of the KSZ effect. This could explain why the better designed UF requires three times larger velocities than the MF to detect the average motion of ~ 700 clusters.

MH, by contrast, used a different approach. Instead of computing the dipole at cluster locations, MH fit dipole templates to their filtered maps. This approach fails in two important respects: (a) MH require that the total number of clusters, their profiles, and extents be known in advance in order to construct the CMB filter, and (b) by matching the same cluster template to the filtered data they are implicitly assuming that all clusters have the same profile and extent in the original as in the filtered data. Hence, changing the profile, number, or extent of clusters changes the filter (and the filtered map, see Fig. 2c for differences when changing the cluster extent). The filter also alters the cluster profile (Fig. 2f,i). Since the information in the filtered maps is distributed differently than their cluster template, the uncertainties of MH's analysis are greatly enlarged.

As both OMCP and MH restricted themselves to smaller apertures than the ones used by KABKE, the dipole measured by us remained hidden in the residual CMB and noise of their filtered maps. However, we have shown that, despite the shortcomings of their filters, they can be used to measure the DF dipole when larger apertures and an adequate normalization are used. The final error bars would be larger, though, than the quoted $130 - 200$ km s^{-1} since we neglected the contribution of CMB residuals, which are less important for the MH and OMCP filters. After removing any TSZ dipole, the final error bar could be more than one order of magnitude smaller than the values quoted by these authors.

4.3. *Prospects with Planck*

The forthcoming Planck data will have a wider frequency coverage, higher resolution, and lower noise levels than WMAP. In Planck's 217 GHz channel the TSZ signal should vanish down to the relativistic corrections to the TSZ terms, eliminating one source of systematic errors for all apertures. The channel has an angular resolution of $5'$ which will allow the inner part of clusters to be resolved out to higher redshift than is possible with WMAP. In addition, Planck's noise levels are smaller. In the first year of operation, the measured HFI in-flight performance is better than what was expected based on the nominal sensitivity requirements. The satellite has shown to be well suited for the blind detection of clusters using the TSZ effect. The first clusters detected by PLANCK include 189 cluster candidates with signal-to-noise larger than 6 (Planck Collaboration. Planck Early Results: The all-sky early Sunyaev-Zeldovich cluster sample, 2011). These SZ clusters are mostly at moderate redshifts (86% are at $z \leq 0.3$) and span over a decade in mass, up to the rarest and most massive clusters with masses above $10^{15} M_{\odot}$. On the negative side, the noise is fairly inhomogeneous and largely dominated by a white-noise component, but containing a $1/f$ contribution that will complicate the analysis. The second major source of systematic error is foreground contamination which may result in significantly larger parts of the microwave sky lost to this analysis.

For the purpose of understanding the effects on filtering, the new data will have several advantages. Planck has measured the profiles of 62 nearby massive clusters (Planck Colaboration. Planck Intermediate Results V, 2012) that can be used to test the efficiency of each filter, define the proper normalization, and determine the calibration coefficient to translate the dipole from temperature to velocity units. Dipoles could be computed at different apertures to check for consistency, and any potential TSZ dipole that restricts our interpretation of the MH dipoles in WMAP data could be subtracted using frequency information. Planck will thus help us to understand if the results derived here using different filters are statistically inconsistent, and/or in conflict with the DF motion; alternatively, the analysis of Planck data might confirm that alternative filters are indeed less efficient than the KAB filter. In the latter case, the inefficiencies could be corrected to show their intrinsic consistency of all the results.

5. CONCLUSIONS.

We have compared the dipoles measured at cluster locations using the filters proposed by OMCP and MH with the results obtained with the KAB filter. *We find that all filters recover dipoles with similar amplitude and/or similar direction.* Since different filters redistribute power differently, we have renormalized the filtered maps consistently in order to compare the measured dipoles. At each frequency, the CMB maps are multiplied by a factor such that the TSZ signal at that frequency over an aperture of radius $5'$ coincides with the measured value in the original WMAP data. This normalization procedure increases the error bars compared with our previous results due to the uncertainties intrinsic to the normalization coefficients.

While the measured dipoles are consistent with each other, they are not fully in agreement. Filters operate differently in ℓ-space and are based on different assumptions. Unlike the KAB filter, the OMCP and MH filters both make assumptions about the profile of electron density and electron pressure. Furthermore, the OMCP filter effectively erases all power below $\ell = 300$. If all clusters had an extent of $\sim 10'$, the OMCP filter would remove half of the dipole signal. This fraction would be even larger if clusters are more extended. Moreover, if the cluster electron-density profile falls off less rapidly from the center than the pressure profile, then the dipole would be erased much more efficiently by the filter than the monopole. This would explain why our renormalization procedure yields dipole amplitudes for the OMCP filter that are much smaller than those obtained with the other two filters. In order to construct the MH filter it is necessary to know the profiles of all the clusters in the sample and their angular extent. Changing the extent from 10 to $15'$ changes the filter in ℓ-space, which makes the conclusions drawn from our tests of this filter rather uncertain. Also, without a specific knowledge of the electron density profile of all clusters, we resorted to assigning equal weight to all clusters in the sample. This overestimates the contribution from less massive and distant clusters compared to the massive and nearby clusters which in reality dominate the signal, an effect which could affect the direction of the measured dipole.

The shortcomings of these filters need to be compared to the performance of the KAB filter which makes no assumption about the cluster profile or extent, but is designed to remove the intrinsic CMB, the largest contaminant (see eq 1) down to the limits imposed by cosmic variance. In addition, the zero-monopole aperture for the KAB filter has a radius of $\lesssim 30'$, much smaller than what is required by the other two filters. Finally, the dipole signal recovered with the KAB filter shows a robust scaling with the central TSZ monopole (or the equivalent X-ray luminosity, Kashlinsky e al 2010), in a clear indication that the dipole is not produced by some random alignments with the residual CMB. These three aspects make the KAB filter the most efficient, and the least affected by the possible systematics intrinsic to the KAB method, amongst the filters suggested so far. Alternative filtering schemes can possibly be designed, but their design must ensure that they increase the S/N of the measurement, not decrease it.

Using the filters designed by OMCP and MH we obtain different results than these authors. In particular, we show that their findings do no disprove the existence of the "Dark Flow". To the contrary, the results obtained with either filter show a reasonable level of consistency with the Dark Flow measurement. The cause of OMCP and MH failing to reach the same conclusion is likely twofold. First, OMCP and MH assumed that clusters have the same extent in the original and in the filtered data, failing to notice that unresolved clusters in WMAP data have a much larger angular size in the filtered maps. By limiting their analysis to smaller apertures, both groups overwhelmed the KSZ signal with the residual CMB and noise in the filtered maps. Second, dipoles need to be computed within apertures of zero monopole, thereby minimizing the contribution from any TSZ dipole. The size of this aperture ranges form $\sim 30'$ to $50'$ and $60'$ for the KAB, OMCP, and MH filters, respectively. Yet, the TSZ monopole is not zero at these large apertures, particularly for the MH filters which, even at 1°, shows monopole residuals close to -4μK.

The forthcoming Planck data will be very useful to clarify the origin, nature, and scale of the Dark Flow dipole measured in the WMAP data. Cluster profiles can be measured individually to determine the effect of filtering on each of the clusters. The Planck frequency coverage would be crucial to remove any TSZ dipole component and, finally, the 217 GHz channel would be important to test for systematics.

FAB acknowledges financial support from the Spanish Ministerio de Educación y Ciencia (grants FIS2009-07238 and CSD 2007-00050). HE gratefully acknowledges funding provided by NASA grant NNX10AJ69G.

REFERENCES

Atrio-Barandela, F., Kashlinsky, A., Kocevski, D. & Ebeling, H. 2008, ApJ, 675, L57
Atrio-Barandela, F., Kashlinsky, A., Ebeling, H., Kocevski, D., Edge, A. 2010, ApJ, 719, 77 (AKEKE)
Birkinshaw, M. 1999, Phys. Rep., 310, 97
Böhringer, H., et al. 2004, A&A, 425, 367
Ebeling, H., Mullis, C. R., & Tully, R. B. 2002, ApJ, 580, 774
Ebeling, H., et al. 1998, MNRAS, 301, 881
Ebeling, H., et al. 2000, MNRAS, 318, 333
Haenhelt, M. G., & Tegmark, M. 1996, MNRAS, 279, 545
Kashlinsky, A. & Atrio-Barandela, F. 2000, Astrophys. J., 536, L67 (KAB)
Kashlinsky, A., Atrio-Barandela, F., Kocevski, D. & Ebeling, H. 2008, ApJ, 686, L49 (KABKE)
Kashlinsky, A., Atrio-Barandela, F., Kocevski, D. & Ebeling, H. 2009, ApJ, 691, 1479
Kashlinsky, A., Atrio-Barandela, F., Ebeling, H., Edge, A., & Kocevski, D. 2010, ApJ, 712, L81
Kashlinsky, A., Atrio-Barandela, F. & Ebeling, H. 2011, ApJ, 732, 1
Kashlinsky, A., Atrio-Barandela, F., Ebeling, H. 2012, Phys. Rep. (submitted). Preprint: arXiv:1202.0717
Kocevski, D. D., et al. 2007, ApJ, 662, 224
Keisler, R. 2009, ApJ, 707, L42
Komatsu, E., & Seljak, U. 2001, MNRAS, 1353
Mak, D. S. Y., Pierpaoli, E., & Osborne, S. J. 2011, ApJ, 736, 116
Mody, K. & Hajian, A. 2012, ApJ, 758, 4 (MH)
Osborne, S. J., Mak, D. S. Y., Church, S. E., & Pierpaoli, E. 2011, ApJ, 737, 98 (OMCP)
Planck Collaboration. Planck Early Results XXVI, 2011, A& A, 536, 26
Planck Collaboration. Planck Early Results: The all-sky early Sunyaev-Zeldovich cluster sample, 2011, A& A, submitted. Preprint, 1101.2024.
Planck Collaboration. Planck Intermediate Results V, 2012, A& A, submitted. Preprint arXiv:1207.4061
Pratt, G. et al. 2011, A&A, 461, 71
Sunyaev, R. A. & Zel'dovich, Y. B. 1970, ApSS, 7, 3
Sunyaev, R. A. & Zel'dovich, Y. B. 1972, CoASP, 4, 173
White, D. A., Jones, C., & Forman, W. 1997, MNRAS, 292, 419

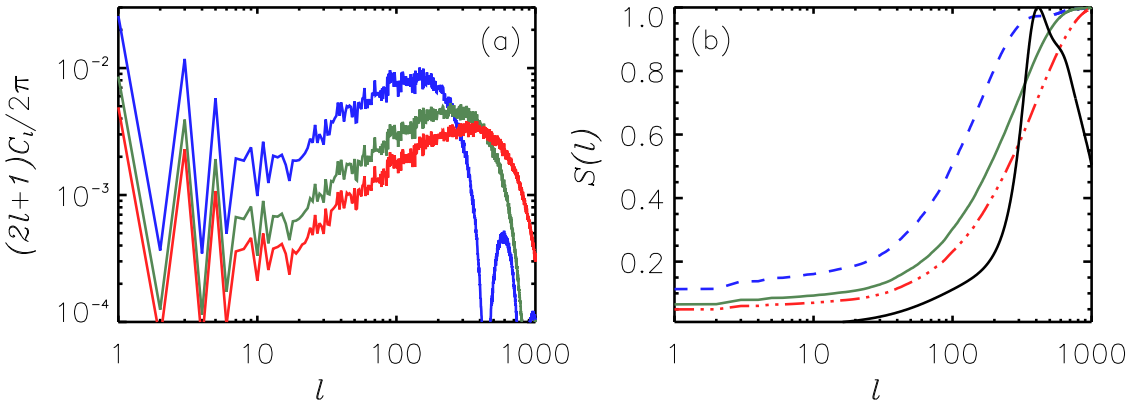

FIG. 1.— Integrated dipole signal as a function of multipole. The dipole is **taken to lie** in the direction of the CMB dipole and is computed from 600 clusters of equal angular extent, located at the positions of real clusters in the sky. In (a) we show the power spectrum for clusters of size $30'$, $15'$ and $10'$ from top to bottom (blue, green, and red lines, respectively). In (b) we plot the **integrated** signal (eq. 2) for the same three angular sizes, with dashed (blue), solid (green) and dot-dashed (red) red lines corresponding to sizes of $30'$, $15'$, and $10'$. For comparison, the black solid line represents the OMCP filter for the W1 DA.

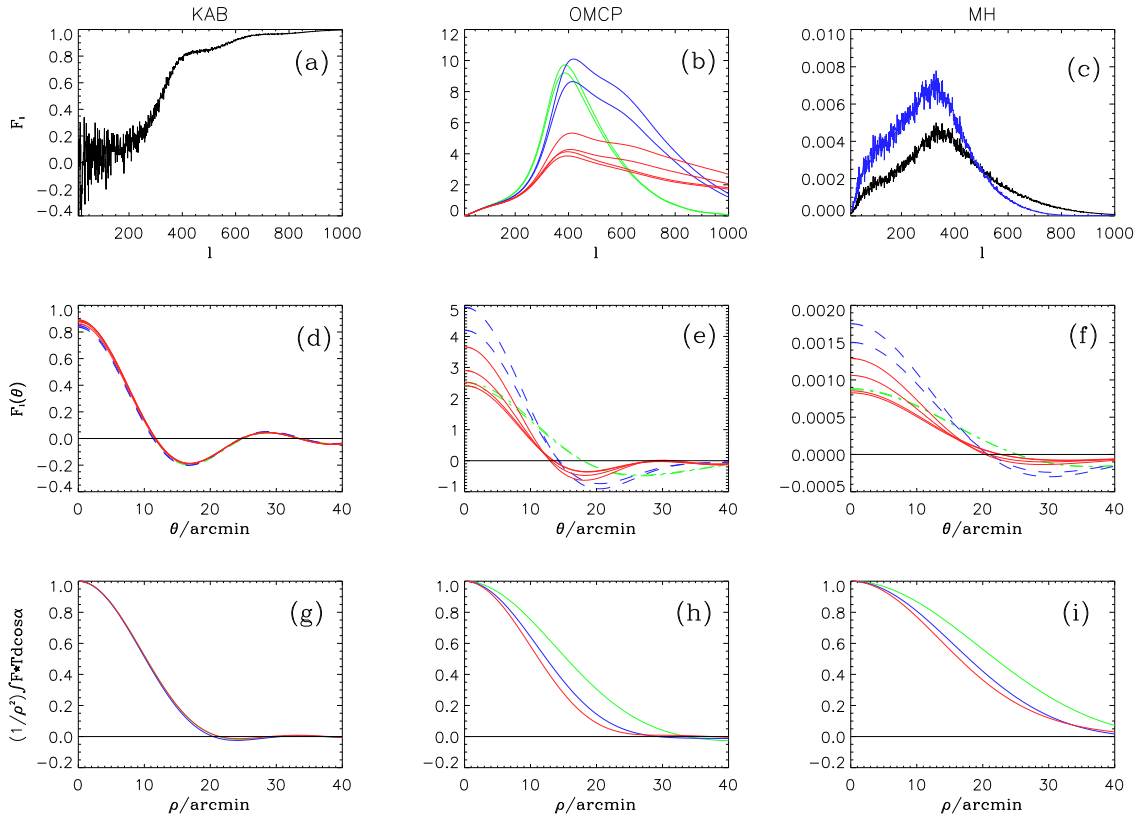

FIG. 2.— Filters in **(top to bottom)** ℓ space, real space, and signal integrated over a disc of angular radius ρ for **(left to right)** the three different filters **defined by** KAB, OMCP, and MH discussed in Sec. 2. (a) KAB filter for the WMAP W1 Differencing Assembly. (b) OMCP filters for the Q (green), V (blue) and W (red) **channel**. (c) MH filters, computed assuming that all clusters have the same angular size of either $10'$ (black line) or $15'$ (blue line). (d–f) The respective filters in real space. Dot-dashed (green), dashed (blue) and solid (red) lines correspond to the Q, V and W bands, respectively (Q1, V1, and W1 for KAB). (g–i) Filter averaged over an aperture of size ρ as a function of aperture size. Lines follow the same convention as in (d–f).

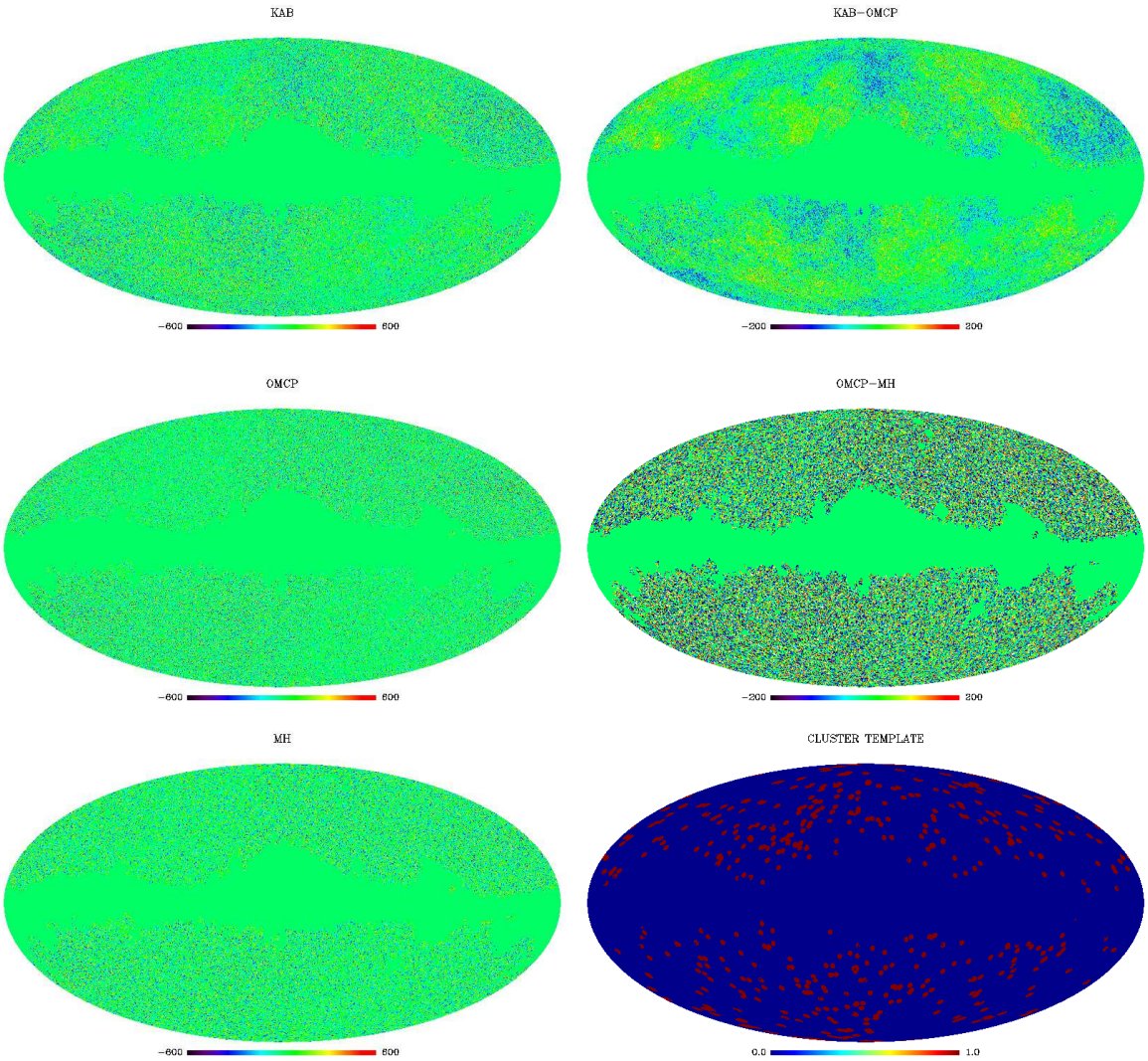

FIG. 3.— Filtered maps and cluster template. Left column and from top to bottom: W1 DA map filtered using the KAB, OMCP and MH filters. Right column: differences between the KAB-OMCP and OMCP-MH filtered maps. Bottom: distribution on the sky of the 480 clusters of our sample. Clusters are ploted as discs of radius 1.5° for easier visualization.

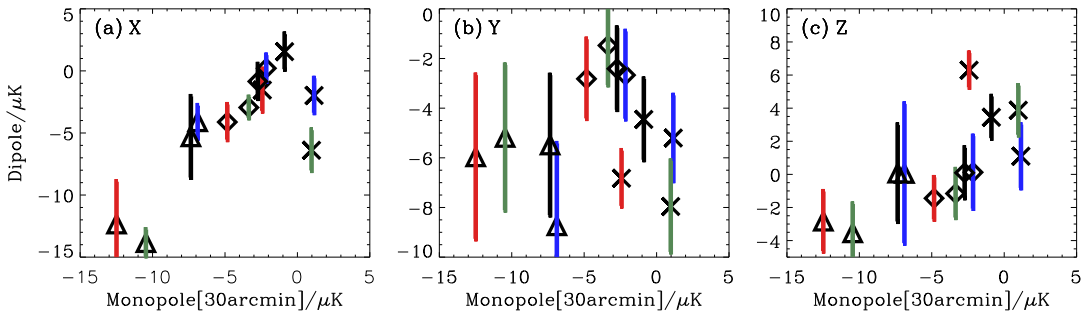

FIG. 4.— Dipole components computed within circles of 30′ radius with corresponding error bars. Crosses, diamonds and triangles correspond to the values measured from W-band maps filtered with the KAB, OMCP, and MH filters. Error bars are the rms dispersion for the four W DA's. Black, blue, red, and green error bars corresponds to the cluster configurations labelled I–IV in Table 1, respectively.

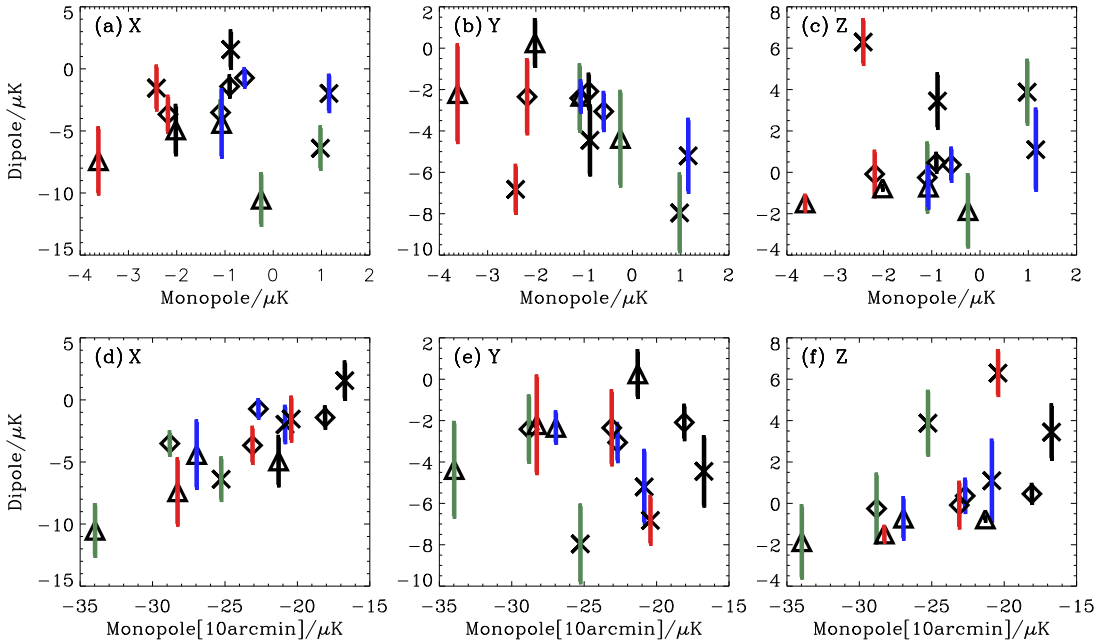

FIG. 5.— Dipole at zero monopole and correlation with X-ray luminosity. In (a–c) we plot the X, Y, and Z components of the dipole, evaluated within 50′ and 60′ apertures for the OMCP (diamonds) and MH (triangles) filters, respectively, versus the monopole at the same aperture. Those apertures correspond to the 'zero monopole' aperture for the respective filters. For comparison, the results of KAB (crosses) at 30′ are also shown. In (d–f) we present the same data with respect to the TSZ monopole measured within apertures of 10′ radius to demonstrate the correlation of the measured dipole with the properties of the cluster sample. Colors denote different cluster configurations as indicated in the caption to Fig. 4.